# SOME INVESTIGATIONS ON DIELECTRIC ROD AERIALS
## Part V

*By* H. R. RAMANUJAM AND (MRS.) R. CHATTERJEE
*(Electrical Communication Engineering Department, Indian Institute of Science, Bangalore-12)*

Received on May 18, 1962

ABSTRACT

An expression for the radiated field intensity from a circular dielectric rod aerial excited in $HE_{11}$ mode has been derived by assuming that the source fields are distributed from both the cylindrical surface and circular end of the rod. Experimental results in support of the theory are also presented.

### INTRODUCTION

In previous reports[1-4] Chatterjee, *et. al.* have formulated theories of radiation pattern from a circular dielectric rod aerial excited in $HE_{11}$ mode. In the scalar formulation,[2] Huyghen's sources were assumed to be distributed all along the surface of the rod, whereas, in the vector formulation,[1] fictitious electric and magnetic charges distributed over the surface of the rod in accordance with Schelkunoff's Equivalence principle[5] were assumed to be responsible for the radiation from the rod. In the formulation,[1] effect of the radiation from the free end of the rod was considered to be insignificantly small compared to the radiation from the surface of the rod and hence the radiation from the end was neglected. Brown and Spector[6] have derived a theory on the assumption that only the infinite plane at the free end of the rod takes part in radiation and the cylindrical surface of the rod acts as a guide to spread the source fields on the infinite plane at the free end of the rod. The object of the present paper is to present a theory of radiation for a circular dielectric rod excited in $HE_{11}$ mode assuming that the source fields exist not only on the cylindrical surface of the rod but also on the free end. Experimental results in confirmation of the theory are reported. It is believed that the same approach can be adopted in calculating the radiation characteristics of a dielectric rod aerial excited in other possible modes.

### FIELD COMPONENTS

The co-ordinate system used is shown in Fig. I. Assuming,

(i) $\partial/\partial z = -\gamma = -j\beta$ where the phase constant $\beta$ is positive and real;

(ii) $\partial^2/\partial\phi'^2 = -1$ as the $HE_{11}$ mode is characterised by a sinusoidal variation of one cycle of the azimuthal angle $\phi'$, and omitting for convenience, the factor exp. $(j\omega t - j\beta z)$, the field components for the $HE_{11}$ mode in the two

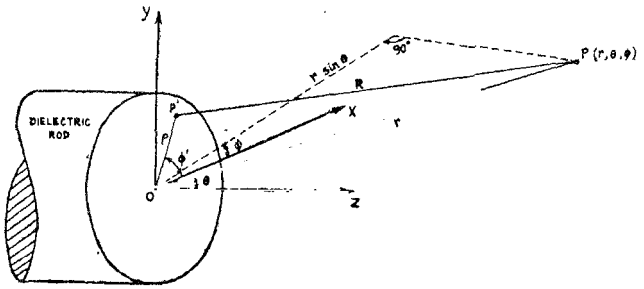


FIG. I
Coordinate systems employed

TABLE FOR TRANSMISSION OF COORDINATES

| | $\hat{x}$ | $\hat{y}$ | $\hat{z}$ |
|---|---|---|---|
| $\hat{r}$ | $\sin\theta\cos\phi$ | $\sin\theta\sin\phi$ | $\cos\theta$ |
| $\hat{\theta}$ | $\cos\theta\cos\phi$ | $\cos\theta\sin\phi$ | $-\sin\theta$ |
| $\hat{\phi}$ | $-\sin\phi$ | $\cos\phi$ | 0 |

| | $\hat{x}$ | $\hat{y}$ | $\hat{z}$ |
|---|---|---|---|
| $\hat{\rho}$ | $\cos\phi'$ | $\sin\phi'$ | 0 |
| $\hat{\phi}'$ | $-\sin\phi'$ | $\cos\phi'$ | 0 |
| $\hat{z}$ | 0 | 0 | 1 |

| | $\hat{r}$ | $\hat{\theta}$ | $\hat{\phi}$ |
|---|---|---|---|
| $\hat{\rho}$ | $\sin\theta\cos(\phi'-\phi)$ | $\cos\theta\cos(\phi'-\phi)$ | $\sin(\phi'-\phi)$ |
| $\hat{\phi}'$ | $-\sin\theta\sin(\phi'-\phi)$ | $-\cos\theta\sin(\phi'-\phi)$ | $\cos(\phi'-\phi)$ |
| $\hat{z}$ | $\cos\theta$ | $-\sin\theta$ | 0 |

media obtained by solving Maxwell's electro-magnetic equations subject only to the boundary conditions on the cylindrical surface of the rod are as follows:

Medium 1: (dielectric rod), $\rho \leq a$

$$E_{z1} = -C G_1 (k_1/\gamma) J_1(k_1 \rho) \sin \phi'$$

$$E_{\rho 1} = C\left[\frac{J_1(k_1 \rho)}{k_1 \rho} + G_1 J_1'(k_1 \rho)\right] \sin \phi'$$

$$E_{\phi' 1} = C\left[J_1'(k_1 \rho) + G_1 \frac{J_1(k_1 \rho)}{k_1 \rho}\right] \cos \phi'$$

$$H_{z1} = \frac{C k_1}{j\omega \mu_1} J_1(k_1 \rho) \cos \phi'$$

$$H_{\rho 1} = -\frac{C\gamma}{j\omega \mu_1}\left[J_1'(k_1 \rho) - G_1 \frac{\omega^2 \mu_1 \epsilon_1}{\gamma^2} \cdot \frac{J_1(k_1 \rho)}{k_1 \rho}\right] \cos \phi'$$

$$H_{\phi' 1} = \frac{C\gamma}{j\omega \mu_1}\left[\frac{J_1(k_1 \rho)}{k_1 \rho} - G_1 \frac{\omega^2 \mu_1 \epsilon_1}{\gamma^2} J_1'(k_1 \rho)\right] \sin \phi' \qquad [1]$$

Medium 2: (space surrounding the dielectric rod) $\rho \geq a$

$$E_{z2} = -D G_2 (k_2/\gamma) H_1^{(1)}(k_2 \rho) \sin \phi'$$

$$E_{\rho 2} = D\left[\frac{H_1^{(1)}(k_2 \rho)}{k_2 \rho} + G_2 H_1^{(1)'}(k_2 \rho)\right] \sin \phi'$$

$$E_{\phi' 2} = D\left[H_1^{(1)'}(k_2 \rho) + G_2 \frac{H_1^{(1)}(k_2 \rho)}{k_2 \rho}\right] \cos \phi'$$

$$H_{z2} = D \frac{k_2}{j\omega \mu_2} H_1^{(1)}(k_2 \rho) \cos \phi'$$

$$H_{\rho 2} = -\frac{D\gamma}{j\omega \mu_2}\left[H_1^{(1)'}(k_2 \rho) - G_2 \frac{\omega^2 \mu_2 \epsilon_2}{\gamma^2} \cdot \frac{H_1^{(1)}(k_2 \rho)}{k_2 \rho}\right] \cos \phi'$$

$$H_{\phi' 2} = \frac{D\gamma}{j\omega \mu_2}\left[\frac{H_1^{(1)}(k_2 \rho)}{k_2 \rho} - G_2 \frac{\omega^2 \mu_2 \epsilon_2}{\gamma^2} H_1^{(1)'}(k_2 \rho)\right] \sin \phi' \qquad [2]$$

where, $a$ is the radius of the dielectric rod

$$k_1^2 = \gamma^2 + \omega^2 \mu_1 \epsilon_1 \; ; \quad k_2^2 = \gamma^2 + \omega^2 \mu_2 \epsilon_2 \qquad [3]$$

To satisfy the conditions at $\rho = 0$ and $\rho = \infty$, Bessel function of the first kind $(J_1)$ and the Hankel function $(H_1^{(1)})$ have been used in the first and second medium respectively. It may also be written that $k_1^2 > 0 > k_2^2$ (Appendix I).

Six of the seven unknowns $C, CG_1, D, DG_2, k_1, k_2$ and $\gamma$ can be determined by using eq. [3] and imposing the following boundary conditions at $\rho = a$

$$E_{z1} = E_{z2} \; ; \quad E_{\phi' 1} = E_{\phi' 2} \; ; \quad H_{z1} = H_{z2} \; ; \quad H_{\phi' 1} = H_{\phi' 2}. \qquad [4]$$

The remaining unknown is determined by the input power. It is found that $\mu_1 G_1 = \mu_2 G_2$. If $\mu_1 = \mu_2$, then $G_1 = G_2 = G$. The propagation constant $\gamma$ is determined as reported elsewhere[1,7].

## Radiated Field due to the Free End of the Rod

The following relations as reported elsewhere[1] have been used to derive a relation for the field intensity at a distant point from the aerial.

$$\mathbf{J} = +\mathbf{n} \times \mathbf{H} \qquad [5]$$

$$\mathbf{M} = -\mathbf{n} \times \mathbf{E} \qquad [6]$$

$$\mathbf{A}^H = \frac{1}{4\pi} \iint \frac{\mathbf{J} \exp.(-jkR)}{R} \, d\Sigma \qquad [7]$$

$$\mathbf{A}^E = \frac{1}{4\pi} \iint \frac{\mathbf{M} \exp.(-jkR)}{R} \, d\Sigma \qquad [8]$$

$$\mathbf{E} = -j\omega \mu_0 \mathbf{A}^H + [1/(j\omega \epsilon_0)] \text{ grad div } \mathbf{A}^H - \text{curl } \mathbf{A}^E \qquad [9]$$

$$\mathbf{H} = -j\omega \epsilon_0 \mathbf{A}^E + [1/(j\omega \mu_0)] \text{ grad div } \mathbf{A}^E + \text{curl } \mathbf{A}^H \qquad [10]$$

where, $\mathbf{n}$ is the unit outward normal to the closed surface $\Sigma$,

$\mathbf{J}$ is the sheet electric current per unit length,

$\mathbf{M}$ is the sheet magnetic current per unit length,

$R$ is the distance from the point $P(\gamma, \theta, \phi)$ to the element of area $d\Sigma$ at $P'(\rho, \phi', z)$,

$\mathbf{A}^H$, $\mathbf{A}^E$ are magnetic and electric vector potentials, respectively.

$k$ is the propagation constant of the medium (free space)

Using the co-ordinate system (Fig. 1) and proper transformation relations, the following expressions for the field components in cartesian co-ordinates in the region $z = 0$, $\rho \leqslant \alpha$ are obtained.

$$E_x = -C(1-G)\sin\phi'\cos\phi'\left[J_1'(k_1\rho) - \frac{J_1(k_1\rho)}{k_1\rho}\right]$$

$$E_y = C\left[J_1'(k_1\rho)(G\sin^2\phi' + \cos^2\phi') + \frac{J_1(k_1\rho)}{k_1\rho}(\sin^2\phi' + G\cos^2\phi')\right]$$

$$H_x = -C'\left[J_1'(k_1\rho)(\cos^2\phi' + G'\sin^2\phi') + \frac{J_1(k_1\rho)}{k_1\rho}(\sin^2\phi' + G'\cos^2\phi')\right]$$

$$H_y = -C'(1-G')\sin\phi'\cos\phi'\left[J_1'(k_1\rho) - \frac{J_1(k_1\rho)}{k_1\rho}\right] \qquad [11]$$

$E_z$ and $H_z$ remain unaltered.

$$C' = \frac{C\gamma}{j\omega\mu_1}, \quad G' = -G\frac{\omega^2\mu_1\epsilon_1}{\gamma^2}$$

$$G \simeq 1 - \frac{\epsilon_r - 1}{\epsilon_r + 1}K_0(k_0 a)(k_0 a)^2$$

$$k_0^2 = \beta^2 - k^2 \qquad \text{[Ref. 6]}$$

where, (Appendix I)

$$G = G' \simeq 1.$$

So, equations [11] reduce to

$$E_x = 0$$

$$H_y = 0$$

$$H_x = -C'\left[J_1'(k_1\rho) + \frac{J_1(k_1\rho)}{k_1\rho}\right] = -C'J_0(k_1\rho)$$

$$E_y = C\left[J_1'(k_1\rho) + \frac{J_1(k_1\rho)}{k_1\rho}\right] = CJ_0(k_1\rho) \qquad [12]$$

Hence,

$$\mathbf{J} = \hat{z} \times \hat{x}\,[-C'J_0(k_1\rho)] = -\hat{y}\,C'J_0(k_1\rho)$$

$$\mathbf{M} = -\hat{z} \times \hat{y}\,[CJ_0(k_1\rho)] = \hat{x}\,CJ_0(k_1\rho) \qquad [13]$$

In order to determine the radiated field ($r >> a \geq \rho$), the distance $R$ given by the following relation

$$R^2 = r^2 - 2r\rho \sin\theta \cos(\phi' - \phi) + \rho^2$$

may be approximated as $R = r$ in the amplitude term, and

$$R = r - \rho \sin\theta \cos(\phi' - \phi)$$

in the phase term of equations [7] and [8].

By expressing $\hat{y}$ in polar co-ordinates and using equations [13] in [7], the following expressions are obtained

$$-j\omega\mu_0 d\mathbf{A}^H = [j\omega\mu_0 C' J_0(k_1\rho)/4\pi r](\hat{r}\sin\theta\sin\phi + \hat{\theta}\cos\theta\sin\phi + \hat{\phi}\cos\phi) \times d\Sigma \exp.[jk\rho\sin\theta\cos(\phi' - \phi) - jkr]$$

$$= [Cj\beta/4\pi r] J_0(k_1\rho)(\hat{r}\sin\theta\sin\phi + \hat{\theta}\cos\theta\sin\phi + \hat{\phi}\cos\phi) \times d\Sigma \exp.[jk\rho\sin\theta\cos(\phi' - \phi) - jkr] \quad [14]$$

where $\mu_1 = \mu_0$

$$\frac{1}{j\omega\epsilon_0} \text{grad div } d\mathbf{A}^H = \frac{k^2 C^1}{j\omega\epsilon_0} \cdot \frac{J_0(k_1\rho)}{4\pi r} \hat{r}\sin\theta\sin\phi\, d\Sigma \times \exp.[jk\rho\sin\theta\cos(\phi' - \phi) - jkr]$$

$$= -[Cj\beta/4\pi r] J_0(k_1\rho)\hat{r}\sin\theta\sin\phi \times d\Sigma \exp.[jk\rho\sin\theta\cos(\phi' - \phi) - jkr] \quad [15]$$

where, terms involving higher powers of $1/r$ have been neglected and

$$k^2 = \omega^2\mu_0\epsilon_0.$$

Expressing $\hat{x}$ in polar co-ordinates and using equations [8] and [13]

$$d\mathbf{A}^E = [C/4\pi r] J_0(k_1\rho)(\hat{r}\sin\theta\cos\phi + \hat{\theta}\cos\theta\cos\phi - \hat{\phi}\sin\phi) d\Sigma \times \exp.[jk\rho\sin\theta\cos(\phi' - \phi) - jkr]$$

$$-\text{curl } d\mathbf{A}^E = (jk/4\pi r) J_0(k_1\rho)(\hat{\theta}\sin\phi + \hat{\phi}\cos\theta\cos\phi)\, d\Sigma \times \exp[jk\rho\sin\theta\cos(\phi' - \phi) - jkr] \quad [16]$$

neglecting terms involving higher powers of $1/r$.

The radiated electric field intensity due to the free end is obtained by substituting equations [14], [15], [16] in [9], as follows

$$\mathbf{E}_1 = (cj/4\pi r)[\hat{\theta}\sin\phi\,(\beta\cos\theta + k) + \hat{\phi}\cos\phi\,(\beta + k\cos\theta)]\exp(-jkr) \times \int_{\rho=0}^{a}\int_{\phi'=0}^{2\pi} \rho\, J_0(k_1\rho)\exp[jk\rho\sin\theta\cos(\phi' - \phi)]\, d\phi'\, d\rho$$

$$= (c_J/4\pi r)[\hat{\theta}\sin\phi\,(\beta\cos\theta + k) + \hat{\phi}\cos\phi\,(\beta + k\cos\theta]\exp(-jkr) \times 2\pi a^2\left[\frac{k_1 a\, J_1(k_1 a)\, J_0(ka\sin\theta) - (ka\sin\theta)\, J_1(ka\sin\theta)\, J_0(k_1 a)}{k_1^2 a^2 - k^2 a^2 \sin^2\theta}\right] \quad [17]$$

The terms $(\beta\cos\theta + k)$ and $(\beta + k\cos\theta)$ correspond to the obliquity factor $(1 + \cos\theta)$ encountered in problems on diffraction. For antennas of practical interest $\beta \simeq k$.

## RADIATED FIELD DUE TO THE CYLINDRICAL SURFACE OF THE ROD

The tangential components on the cylindrical surface of the rod ($\rho = a$) are

$$E_z = C_1\sin\phi'\exp.(-j\beta z) \qquad H_z = C_3\cos\phi'\exp.(-j\beta z)$$

$$E_{\phi'} = C_2\cos\phi'\exp.(-j\beta z) \qquad H_{\phi'} = C_4\sin\phi'\exp.(-j\beta z)$$

where

$$C_1 = jC[k_1/\beta]\, G\, J_1(k_1 a) \qquad C_3 = C[k_1/j\omega\mu_1]\, J_1(k_1 a)$$

$$C_2 = C\left[J_1'(k_1 a) + G\frac{J_1(k_1 a)}{k_1 a}\right] \qquad C_4 = -\frac{C\beta}{\omega\mu_0}\left[G' J_1'(k_1 a) + \frac{J_1(k_1 a)}{k_1 a}\right]$$

So,

$$\mathbf{J} = \hat{\rho}\times(\hat{z}\, C_3\cos\phi' + \hat{\phi}'\, C_4\sin\phi')\exp.(-j\beta z)$$
$$= (-\hat{\phi}'\, C_3\cos\phi' + \hat{z}\, C_4\sin\phi')\exp.(-j\beta z)$$

$$\mathbf{M} = -\hat{\rho}\times(\hat{z}\, C_1\sin\phi' + \hat{\phi}'\, C_2\cos\phi')\exp.(-j\beta z)$$
$$= (\hat{\phi}'\, C_1\sin\phi' - \hat{z}\, C_2\cos\phi')\exp.(-j\beta z)$$

In spherical polar co-ordinates, the above expressions for $\mathbf{J}$ and $\mathbf{M}$ reduce to

$$\mathbf{J} = \hat{r}[C_3\sin\theta\cos\phi'\sin(\phi' - \phi) + C_4\cos\theta\sin\phi']\exp.(-j\beta z) + \hat{\theta}[C_3\cos\theta\cos\phi'\sin(\phi' - \phi) - C_4\sin\theta\sin\phi']\exp.(-j\beta z) + \hat{\phi}[-C_3\cos\phi'\cos(\phi' - \phi)]\exp.(-j\beta z) \quad [18]$$

$$\mathbf{M} = \hat{r}\,[-C_1 \sin\theta \sin\phi' \sin(\phi' - \phi) - C_2 \cos\theta \cos\phi'] \exp.(-j\beta z)$$
$$+ \hat{\theta}[-C_1 \cos\theta \sin\phi' \sin(\phi' - \phi) + C_2 \sin\theta \cos\phi'] \exp.(-j\beta z)$$
$$+ \hat{\phi}[C_1 \sin\phi' \cos(\phi' - \phi)] \exp(-j\beta z) \qquad [19]$$

The distance between an element of area $a\,d\phi'\,dz$ at $(a, \phi', z)$ and a point at $(r, \theta, \phi)$ is

$$R^2 = r^2 - 2ra \sin\theta \cos(\phi' - \phi) - 2r \cos\theta \cdot z + a^2 + z^2$$

For the radiated field $r >> a$, $r >> 1 \geq |z|$. So, in the phase and amplitude terms of equations [7] and [8] $R$ can be approximated by

$$R = r - a \sin\theta \cos(\phi' - \phi) - z \cos\theta$$

and $R = r$ respectively.

So, from equations [7] and [18], [8] and [19]

$$-j\omega\mu_0\, d\mathbf{A}^H = (j\omega\mu_0/4\pi r)\,\mathbf{J}\,d\Sigma \exp.[ju\cos(\phi' - \phi) + jkz\cos\theta - jkr]$$

$$(1/j\omega\epsilon_0)\,\text{grad div}\,\mathbf{A}^H = (j\omega\mu_0/4\pi r)\,\hat{r}\,J_r\,d\Sigma \exp.[ju\cos(\phi' - \phi) + jkz\cos\theta - jkr]$$

$$-\text{curl}\,d\mathbf{A}^E = (-jk/4\pi r)(\hat{\theta}M_\phi - \hat{\phi}M_\theta)d\Sigma \exp.[ju\cos(\phi' - \phi) + jkz\cos\theta - jkr] \qquad [20]$$

The radiated field due to the cylindrical surface of the rod is obtained by substituting equations [18], [19] and [20] in [9]

$$\mathbf{E}_2 = -\frac{j}{4\pi r}\int_{z=-l}^{0}\int_{\phi'=0}^{2\pi}[\hat{\theta}(\omega\mu_0 J_\theta + kM_\phi) + \hat{\phi}(\omega\mu_0 J_\phi - kM_\theta)]$$
$$\times \exp.[ju\cos(\phi' - \phi) + jkz\cos\theta - jkr]\,a\,d\phi'\,dz$$

which yields

$$\mathbf{E}_2 = -\frac{ja}{4r}\Bigg[\hat{\theta}\sin\phi\Big\{J_0(u)[kC_1 - \omega\mu_0 C_3\cos\theta] - J_2(u)[kC_1 + \omega\mu_0 C_3\cos\theta] - \frac{2\omega\mu_0 C_4}{ka}juJ_1(u)\Big\}$$
$$+\hat{\phi}\cos\phi\Big\{J_0(u)[-\omega\mu_0 C_3 + kC_1\cos\theta] + J_2(u)[\omega\mu_0 C_3 + kC_1\cos\theta] - \frac{2C_2 juJ_1(u)}{a}\Big\}\Bigg]$$
$$\times l\exp.(jx - kr)(\sin x/x) \qquad [21]$$

where, $u = ka\sin\theta$ ; $x = \frac{1}{2}(\beta - k\cos\theta)$ ; $l$ = length of the dielectric rod.

Numerical calculations show that $k C_1 \simeq -\omega \mu_0 C_3$. So, the terms $k C_1 - \omega \mu_0 C_3 \cos\theta$ and $-\omega \mu_0 C_3 + k C_1 \cos\theta$ correpond to the obliquity factor, $1 + \cos\theta$.

## RADIATION PATTERN

As the magnitude of the total field $E$ is of interest for the radiation pattern, the resultant field $E$ due to the contribution from the end $f_1 f_2$ as well as the cylindrical surface $f_3 f_4$ of the rod is obtained from equations [17] and [21] as follows after omitting the factor $(j a C/4r) \exp.(j\omega t - kr)$

$$E = f_1 f_2 + f_3 f_4 \qquad [22]$$

where,

$$f_1 = \beta + k\cos\theta \text{ in } \phi = 0^\circ \text{ plane, and}$$

$$= \beta \cos\theta + k \text{ in } \phi = \pi/2 \text{ plane} \qquad [a]$$

$$f_2 = 2a \frac{k_1 a J_1(k_1 a) J_0(u) - u J_1(u) J_0(k_1 a)}{k_1^2 a^2 - u^2} \qquad [b]$$

$$f_3 = \frac{1}{jC}\Big[J_0(u)(-\omega\mu_0 C_3 + k C_1 \cos\theta) + J_2(u)(\omega\mu_0 C_3 + k C_1 \cos\theta) - 2C_2 \frac{j u J_1(u)}{a}\Big] \text{ in } \phi = 0^\circ \text{ plane}$$

and

$$= \frac{1}{jC}\Big[J_0(u)(k C_1 - \omega\mu_0 C_3 \cos\theta) - J_2(u)(k C_1 + \omega\mu_0 C_3 \cos\theta) - \frac{2\omega\mu_0 C_4}{k a} j u J_1(u)\Big] \text{ in } \phi = \frac{\pi}{2} \text{ plane} \qquad [c]$$

and

$$f_4 = l \exp.\left(jx - \frac{\pi}{2}\right) \frac{\sin x}{x} \qquad [d]$$

It is observed that $f_1$, $f_2$, $f_3$ are functions of the diameter $d = 2a$ and dielectric constant $\epsilon$ of the rod, and $f_4$ is a function of d, $\epsilon$ and $l$ of the rod. Hence $E$ is a function of $l$, $d$, $\epsilon$ of the rod. Moreover, $f_2$ and $f_3$ can be regarded as array factors due to the finite thickness of the rod and $f_4$ represents the array factor due to the linear dimension of the rod. $f_1$ represents the obliquity factor, but it is slightly different from the corresponding factor $1 + \cos\theta$, given in the theory of Brown and Spector,[6] because of the difference in propagation constant, as in the present theory $f_1$ is a function of the propagation constant of the surface wave and depends on $d$ and $\epsilon$ of the rod. Whereas, $f_2$ appears with

an additional term in Brown and Spector's theory as the aperture is considered to be of infinite extent unlike in the present approach. The present theory gives rise to the additional term $f_3$ which takes into account the finite thickness of the rod. It is this factor which gives rise to the difference in the radiation pattern in the $\phi = 0$ and $\phi = \pi/2$ planes which is expected due to the asymmetric field distribution of the $HE_{11}$ mode. The term $f_4$ is the same as obtained through other approaches.

The variation of $f_1$ $f_2$ and $f_3$ with $\theta$ for a rod having $d/\lambda_0 = 0.51$ and $\epsilon = 2.62$ is shown in Figs II and III. The variation of $f_4$ with $\theta$ is well known from previous theories and hence is omitted. It is seen from the graphs that the major lobe about $\theta = 0^\circ$ is sharper in the $\phi = \pi/2$ plane than in the $\phi = 0^\circ$ plane and the side lobes are more prominent in the $\phi = \pi/2$ plane.

The following observations on the effects of varying the parameters on the genaral tendency of the radiation pattern based on equation (22) may be made.

(*i*) The radiation pattern is symmetrical about the axis of the rod.

(*ii*) The pattern in the $\phi = \pi/2$ plane is sharper than in the $\phi = 0^\circ$ plane in the neighbourhood of the axis ($\theta = 0^\circ$) due to the fact that $f_1$ and $f_3$ vary more rapidly with $\theta$ in the $\phi = \pi/2$ plane than in the $\phi = 0^\circ$ plane.

(*iii*) While $f_1$, $f_2$ and $f_3$ are real, $f_4$ is complex with its phase rapidly varying with $\theta$ (Appendix I). The number of lobes are mostly determined by $f_4$.

(*iv*) Increase in $d$ or $\epsilon$ of the rod has the effect of increasing the propagation constant of the surface-wave. This may be responsible for increasing the number of lobes, their levels and back radiation. The pattern is also made sharper.

(*v*) For short lengths ($x < \pi$), increase in the length of the rod has the effect of making the main lobe narrower and increasing the number and levels of the side lobes.

## Experimental

The two main assumptions made in deriving the present theory of radiation were as follows:

(*i*) The expressions for the source felds have been derived by solving Maxwell's equations with proper boundary conditions but ignoring radiation from the rod.

(*ii*) Radiation takes place from the free end of the rod.

Experiments have been conducted to justify the first assumption by (*a*) comparing the experimentally determined propagation constant of the surface wave with that calculated from the theory, and (*b*) comparing the measured radial electric field spread with that predicted from the theory.

The second assumption is sought to be verified by comparing the observed change in the radiated field at a point on the axis with that predicted from the theory, when radiation from the free end is supressed by covering it with metal foils of different size.

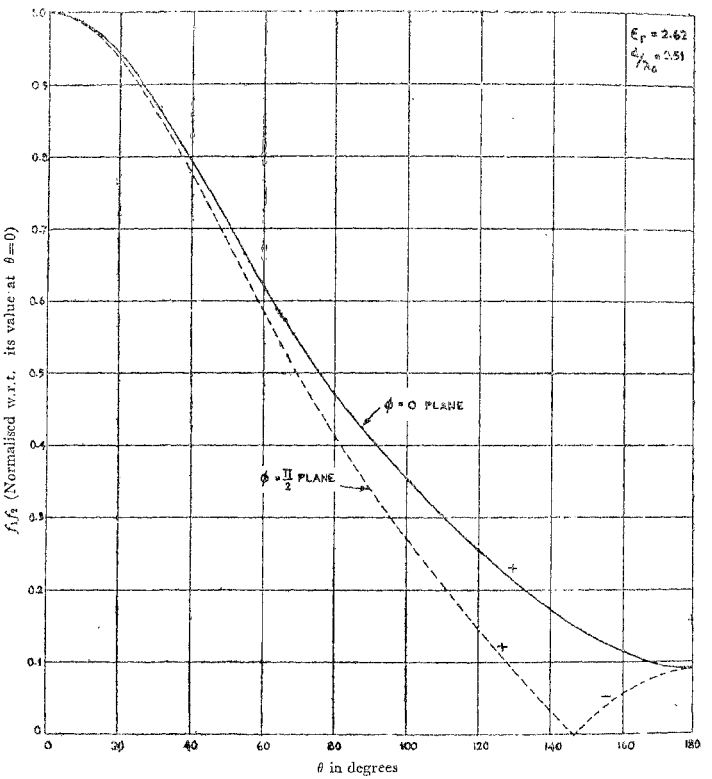


FIG. II
Variation of $f_1 f_2$ with $\theta$

Experiments have also been conducted to determine the transmission of power inside ($P_i$) the rod compared to the power flowing outside ($P_0$) the rod.

The experimental set up for the determination of propagation constant, radial field spread and the radiated field intensity at a distant point on the axis

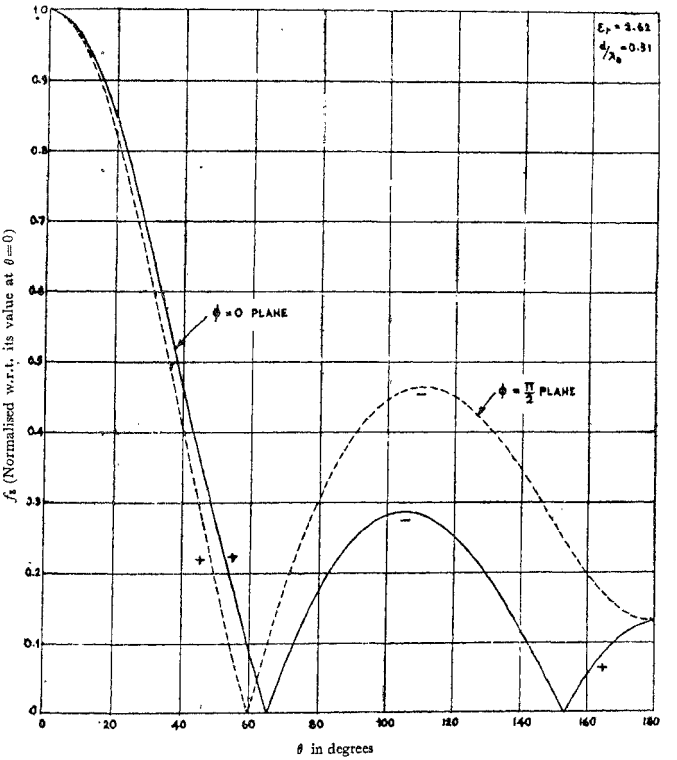


FIG. III

Variation of $f_s$ with $\theta$

of the rod is shown in the block schematic diagrams of Fig. IV and in Plate I, II and III. A close up of the probe carriage is shown in Plate IV. The sketch of the dielectric rod acrial with metal discs and rings is shown in Fig. V.

(*a*) *Determination of the propagation constant*:—The description of the dielectric rods employed in experiments is given in Appendix II. The field

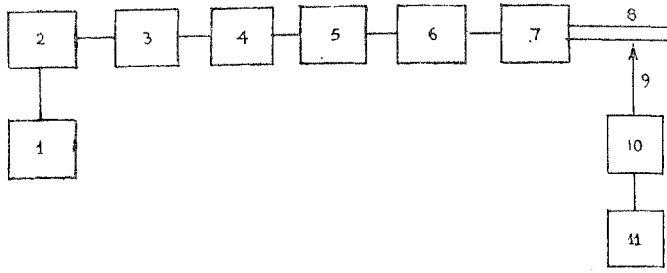


(*a*) Measurement of field near the dielectric rod

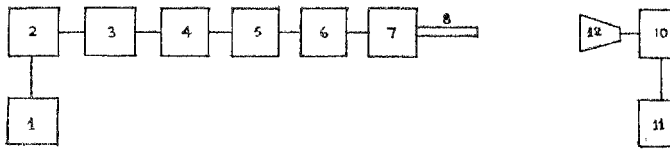


(*b*) Measurement of radiated field

1. Universal Klystron Power Supply. P.R.D. Type 801-A, No. 795
2. Microwave Oscillator. 723 A/B Klystron, Western Electric
3. Buffer Attenuator. 0-20 db. P.R.D. Type 160-A, No. 106
4. Frequency Meter. 8.2—10 KMc/s. P.R.D. Type 558-A, No. 128
5. Precision Attenuator. P.R.D. Type 160-A, No. 107
6. Buffer Attenuator. 0-20 db. P.R.D. Type 160-A, 107
7. *Mode Transformer
8. Dielectric Rod Acrial
9. Probe. P.R.D. Type 250-A, No. 2105 (Mounted on *Probe Carriage)
10. Detector IN23B Crystal
11. *Detector Amplifier
12. *Pyramidal Horn

*Constructed in the Laboratory

FIG. IV

Block schematics of the experimental setup

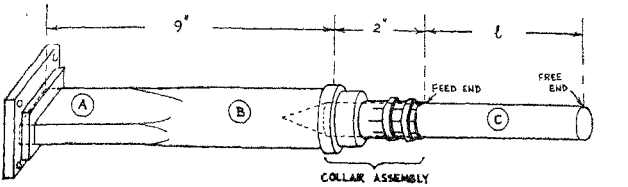


(a) DIELECTRIC ROD FITTED TO THE MODE TRANSFORMER

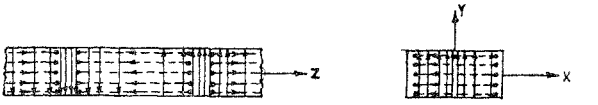


(b) FIELD CONFIGURATION AT (A) $H_{10}$ MODE

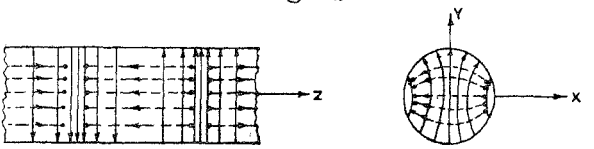


(c) FIELD CONFIGURATION AT (B) $H_{11}$ MODE

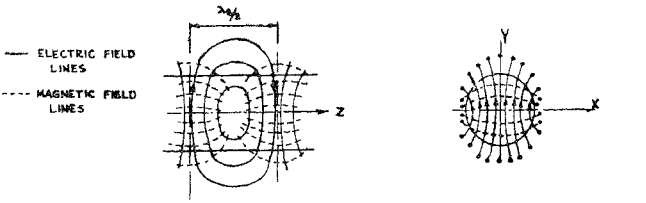


(d) FIELD CONFIGURATION AT (C) $HE_{11}$ MODE

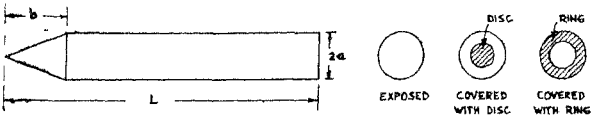


(e) DIELECTRIC ROD END VIEWS

FIG. V

Sketch of dielectric rod aerial with field configurations

distributions near the rods for all the dielectric rods have been measured in terms of the calibrated precision attenuator. The power standing wave distribution ($E_p^2$) for the perspex rod $B_2$ near the feed end, middle region and the free end are shown in Figs. VI, VII and VIII, both for the free end fully covered with a tin foil disc and for the case of the free end fully exposed. It is to be noted that the units for $E_p^2$ are not the same for the three figures presented, as the height of the tip of the probe above the surface might have been different in the three regions. It is observed that the field distribution is irregular for a distance of about a wavelength from the feed end of the rod. This is to be expected because the additional boundary condition to be satisfied at the junction of the rod and the mode transformer would require the presence of higher order modes which have not been taken into account in deriving the source fields. In the middle region, however, the fields distribution is regular and the guide wavelength ($\lambda_g$) was determined in this region. It is also seen that $\lambda_g$ is not altered by covering the free end with tin foil. The position of maxima of field in one case corrpond to those of minima of the other, showing that the reflection coefficients in the two cases are 180° out of phase. The field distribution is again irregular near the free end, beyond which the field remains constant in mangnitude, at the minimum in the case of covered end and at the maximum in the case of the exposed end, The theoretical[7] and experimental values of the propagation constant $\lambda_g$ for rods of different diameter and dielectric constants are given in the following tables.

TABLE I

Propagation constant for rods of different diameters

$\epsilon=2.62$ ; $\lambda_0=3.11$ cms.

| Rod No. | $2a/\lambda_0$ | Theoretical | | Experimental | |
|---|---|---|---|---|---|
| | | $\beta/k=\lambda_0/\lambda_g$ | $\lambda_g$ (cm) | $\beta/k=\lambda_0/\lambda_g$ | $\lambda_g$ (cm) |
| $B_1$ | 0.41 | 1.11 | 2.80 | 1.07 | 2.90 |
| $B_2$ | 0.51 | 1.20 | 2.59 | 1.22 | 2.55 |
| $B_3$ | 0.61 | 1.29 | 2.41 | 1.29 | 2.42 |
| $B_4$ | 0.71 | 1.37 | 2.27 | 1.30 | 2.40 |
| $B_5$ | 0.82 | 1.42 | 2.19 | 1.39 | 2.24 |

Theoretical[7] and experimental variation of $\beta/k$ with $d$ and $\epsilon$ are shown in Fig. IX. The agreement between the theoretical and experimental values is fairly close.

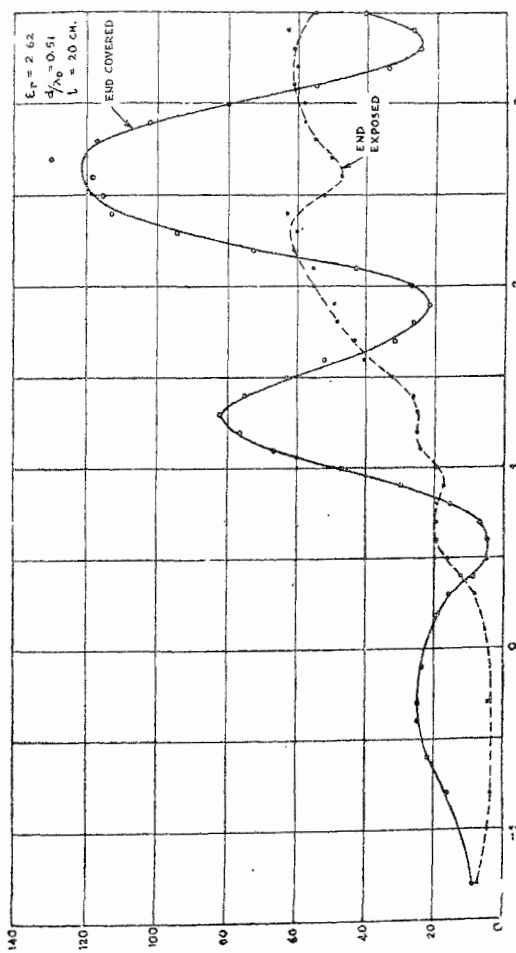


FIGURE VI

Field distribution near the feed end of the dielectric rod $B_2$

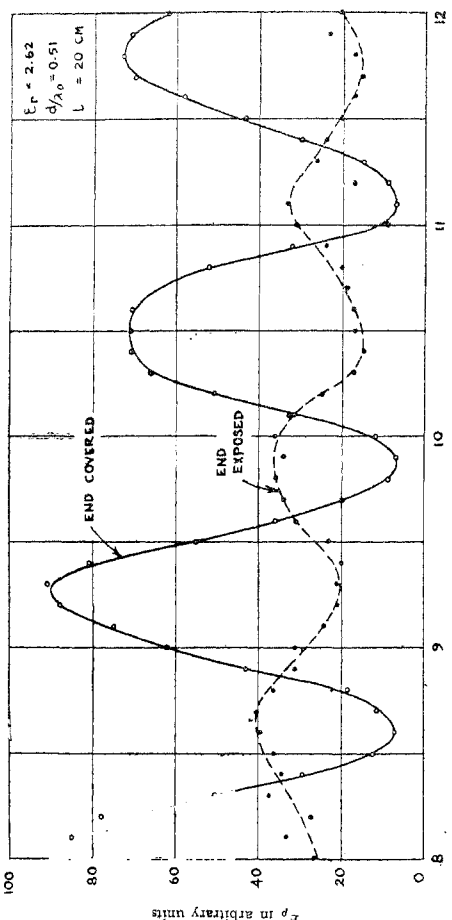


FIG. VII

Field distribution near the middle of the rod $D_0$

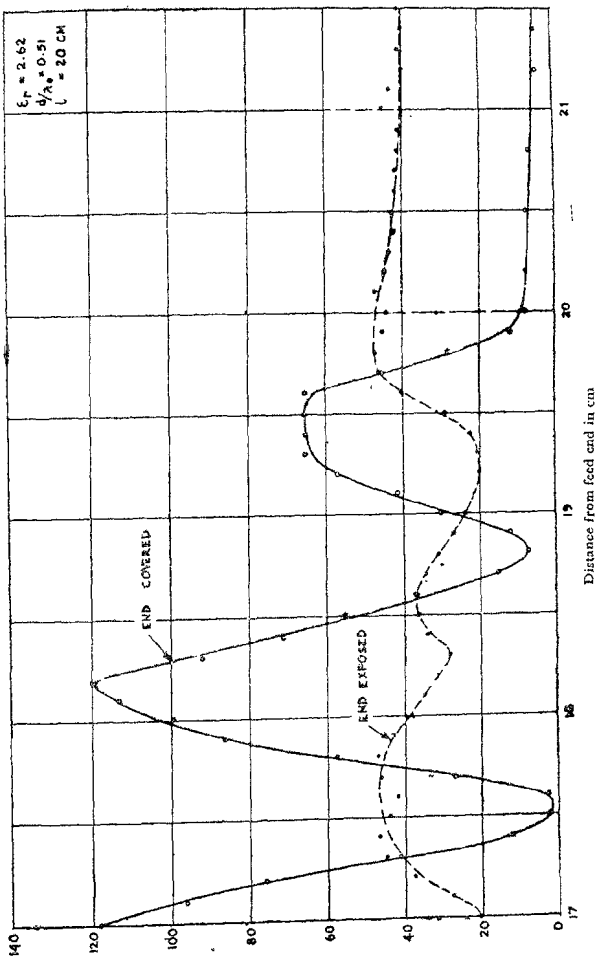


FIG. VIII

Field distribution near the free end of the rod $B_2$

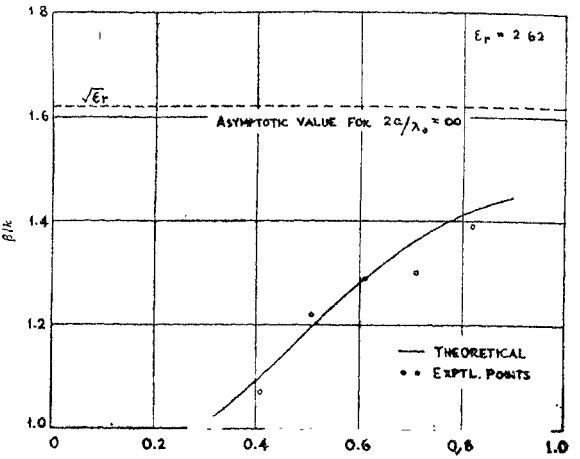


(*a*) Different diameters

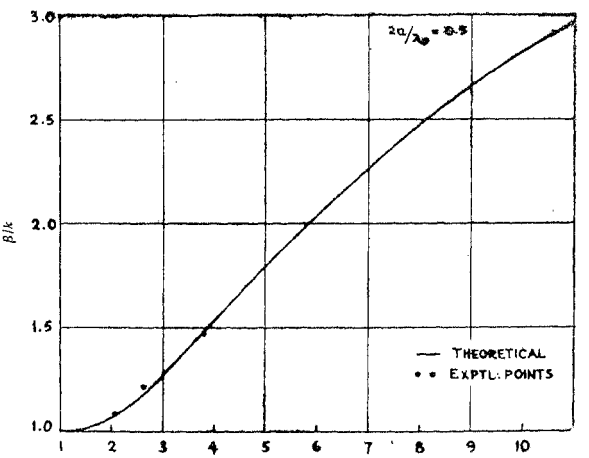


(*b*) Different dielectric constants

FIG. IX

Variation of propagation constant ($\beta$)

TABLE II

Propagation constant for rods of different dielectric constants
$2a/\lambda_0 = 0.51$ ; $\lambda_0 = 3.11$ cms.

| Rod No. | $\epsilon_r$ | Theoretical (values are for $2a/\lambda_0 = 0.50$) | | Experimental | |
|---|---|---|---|---|---|
| | | $\beta/k$ | $\lambda_g$ (cm) | $\beta/k$ | $\lambda_g$ (cm) |
| A | 2.05 | 1.08 | 2.88 | 1.08 | 2.88 |
| $B_2$ | 2.62 | 1.19 | 2.62 | 1.22 | 2.55 |
| C | 3.80 | 1.48 | 2.10 | 1.48 | 2.10 |

(*b*) *Transmission of power through the dielectric rod*:—The v.s.w.r. (S) was determined experimentally both for the case of covered free end and exposed free end for different dielectric rods. The fraction of the input power that is reflected ($P_R$) and that is transmitted ($P_T$) have been calculated by the following relations given by transmission line theory.

$$P_R = [(S-1)/(S+1)]^2$$
$$P_T = 1 - P_R = 4/(2 + 1/S + S)$$

Assuming that the metal disc at the free end fully reflects the power flowing within the rod ($P_i$) leaving the power flowing outside the rod ($P_0$)

TABLE III

V.S.W.R. and power flow through perspex rods of different diameters
$\epsilon = 2.62$ ; $\lambda_0 = 3.11$ cms.

| Rod No. | $2a/\lambda_0$ | End exposed | | | End fully covered | | | $P_i/P_0$ | |
|---|---|---|---|---|---|---|---|---|---|
| | | v.s.w.r. | $P_R$% | $P_T$% | v.s.w.r. | $P_R$% | $P_T$% | Expl. | Theoretical |
| $B_1$ | 0.41 | 1.19 | 0.75 | 99.2 | 3.7 | 33 | 67 | 0.49 | 0.55 |
| $B_2$ | 0.51 | 1.36 | 2.3 | 97.7 | 4.4 | 40 | 60 | 0.67 | 1.66 |
| $B_3$ | 0.61 | 1.33 | 2.0 | 98.0 | 4.9 | 44 | 56 | 0.79 | 3.5 |
| $B_4$ | 0.71 | 1.35 | 2.2 | 97.8 | 4.2 | 38 | 62 | 0.61 | 6.0 |
| $B_5$ | 0.82 | 1.61 | 5.5 | 94.5 | 5.8 | 50 | 50 | 1.00 | 9.0 |

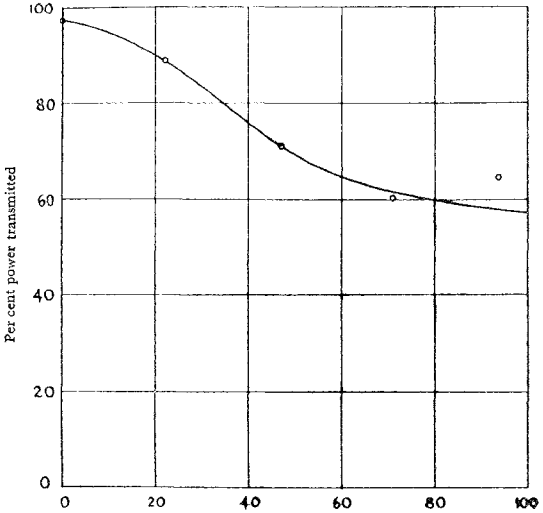


(*a*) Discs

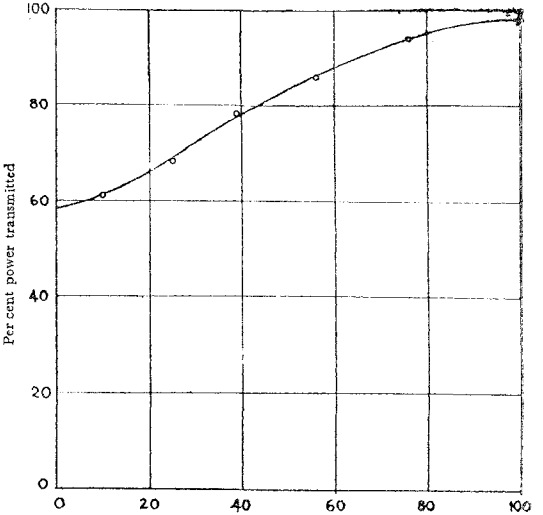


(*b*) Rings

FIG. X

Effect of covering the free end of the rod $B_2$ on the transmission of power

unaltered, the ratio of the two powers is calculated by the relation $P_i/P_0 = P_R/P_T$, where, $P_R/P_T$ is calculated from the v.s.w.r. measured with the free end of the rod covered. The results are presented in Tables III and IV.

TABLE IV

V.S.W.R. and power flow through rods of different dielectric constants

$2a/\lambda_0 = 0.5$, $\lambda_0 = 3.11$ cms.

| Rod No. | $\epsilon$ | End Exposed | | | End fully covered | | | $P_i/P_0$ | |
|---|---|---|---|---|---|---|---|---|---|
| | | v.s.w.r. | $P_R$% | $P_T$% | v.s.w.r. | $P_R$% | $P_T$% | Exp. | Theoretical |
| A | 2.05 | 1.12 | 0.32 | 99.68 | 1.61 | 5.5 | 94.5 | 0.06 | 0.6 |
| $B_2$ | 2.62 | 1.36 | 2.3 | 97.7 | 4.4 | 40 | 60 | 0.67 | 1.6 |
| C | 3.80 | 1.74 | 7.3 | 92.70 | 3.9 | 35 | 65 | 0.54 | 3.5 |

The theoretical values of $P_i/P_0$ were obtained by approximate interpolation from graphs published elsewhere.[8] It is seen that the difference between the theoretical and experimental values of $P_i/P_0$ is too great to be caused by an experimental error or due to interpolation from graphs. It is believed that the discrepancy may be due to the fact that the finite dielectric rod which has been regarded as a simple non-radiating transmission line in the theoretical calculation of $P_i/P_0$ is not justified.

(*iii*) *Effect of covering different areas of the free end on the v.s.w.r.* :—The effect of covering the free end with metal discs and rings on the percentage of power transmitted ($P_T$) and reflected ($P_R$) is shown in Tables V and VI. The discs and rings employed are described in Appendix III. The experiment was conducted with the perspex rod $B_2$ ($2a = 1.60$ cms.). The variation of $P_T$% with respect to the percentage area of the end covered and end exposed is shown in FIG. X.

The radiated power along the axis of the rod, discussed in a later section is given here for the sake of comparison.

RADIATED FIELD SPREAD OUTSIDE THE DIELECTRIC ROD

The radiated field spread is calculated from the following relation

$$\underset{(\phi' = \pi/2)}{E_\rho} = K_0(k_0\rho) + (1 - G)\frac{K_1(k_0\rho)}{k_0\rho}$$

TABLE V

Effect of covering the free end of the rod on the transmission of power Rod $B_2$

Length exposed $l$=20 cms. $\lambda_0$=3.11 cms.

A (Discs)

| Disc. No. | Per cent area of end covered | Distance of minimum from the free end (cms) | V.S.W.R. | $P_R$ | $P_T$% | Radiated power along axis |
|---|---|---|---|---|---|---|
| Exposed | 0 | 8.2 | 1.36 | 2.3 | 97.7 | 100 |
| 1 | 22 | 7.9 | 2.0 | 11 | 89 | 100 |
| 2 | 47 | 7.6 | 3.3 | 26 | 71 | 76 |
| 3 | 71 | 7.6 | 4.4 | 40 | 60 | 67 |
| 4 | 94 | 7.6 | 3.9 | 35 | 65 | 58 |

TABLE VI

B (Rings)

| Ring No. | Per cent area of the end exposed | Distance of minimum from the free end (cms) | V.S.W.R. | $P_R$ % | $P_T$ % | Radiated power along the axis % |
|---|---|---|---|---|---|---|
| Fxposed | 100 | 8.2 | 1.36 | 2.3 | 97.7 | 100 |
| 1 | 77 | 7.1 | 1.7 | 7 | 93 | 93 |
| 2 | 56 | 7.3 | 2.2 | 14 | 86 | 81 |
| 3 | 39 | 7.4 | 2.7 | 21 | 79 | 63 |
| 4 | 25 | 7.45 | 3.6 | 32 | 68 | 63 |
| 5 | 10 | 7.6 | 4.3 | 39 | 61 | 56 |

where, $K_0$ and $K_1$ represent modified Bessel functions of the second kind and order zero and unity respectively. The theoretical and experimental results for the variation of the radial electric field spread for different diameters and dielectric constants are shown in Figs. XI to XIV. The agreement is fairly good.

It may therefore be concluded that the field distribution in the neighbourhood of the dielectric rod conforms to the pattern of the $HE_{11}$ mode as assumed.

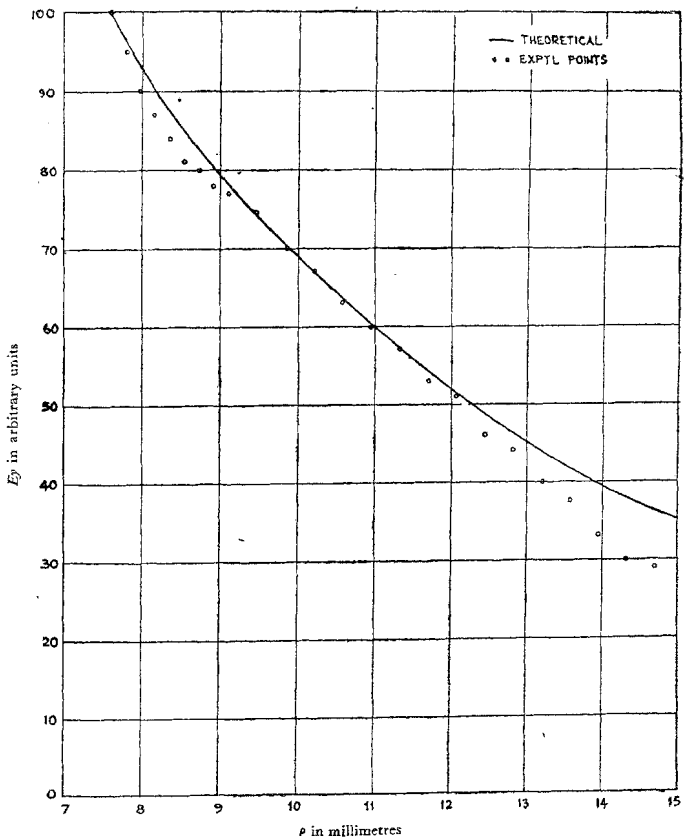


FIG. XI

Field spread outside the dielectric rod $B_1$
$\epsilon_r = 2.62$, $2a/\lambda_0 = 0.41$

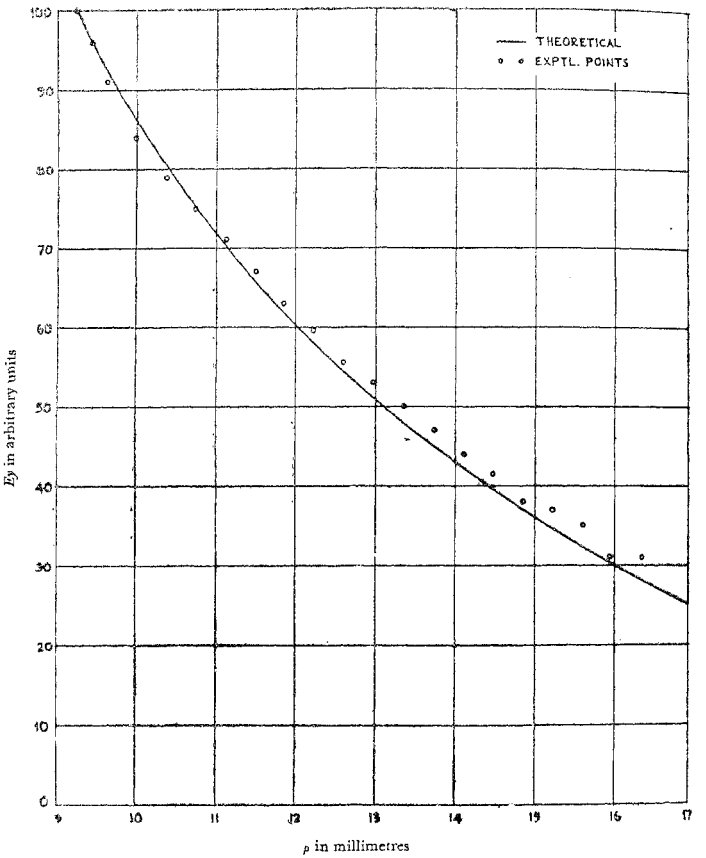


FIG. XII

Field spread outside the dielectric rod $E_z$

$\epsilon_r = 2.62$, $2a/\lambda_0 = 0.51$

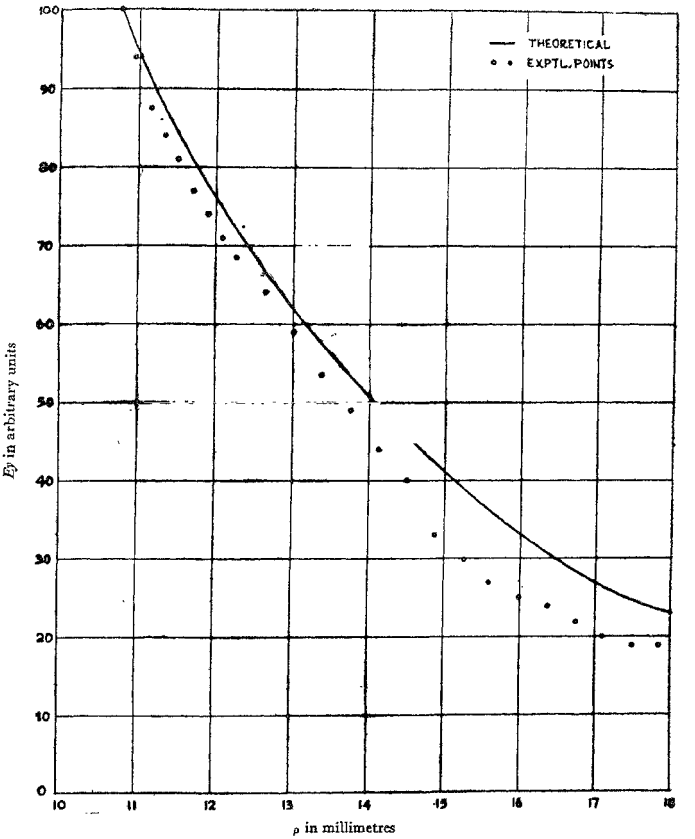


FIG. XIII

Field spread outside the dielectric rod $B_3$

$\epsilon_r = 2.62$, $2a/\lambda_0 = 0.61$

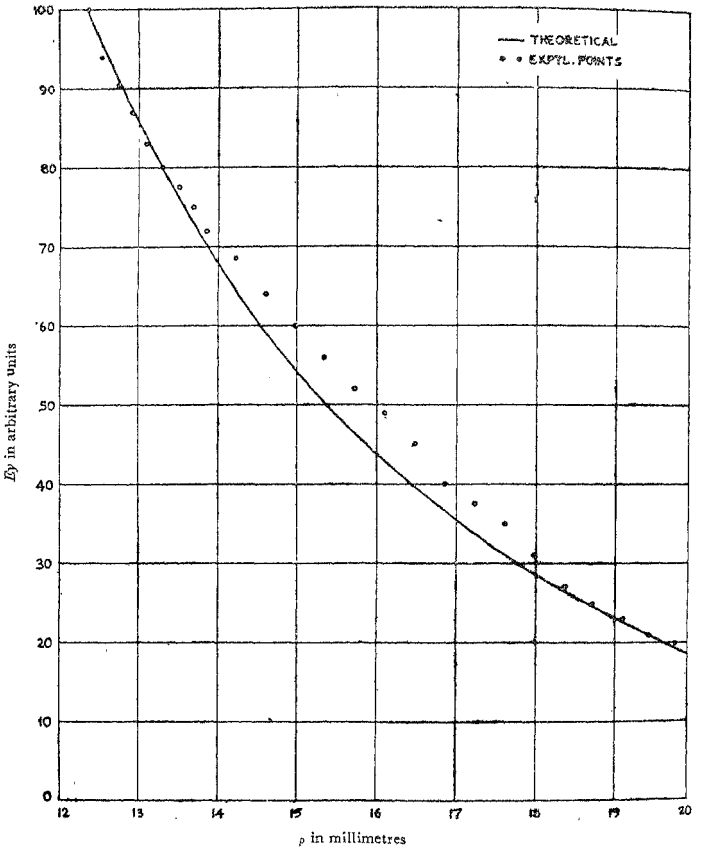


FIG. XIV

Field spread outside the dielectric rod $B_4$

$\epsilon_r = 2.62$, $2a/\lambda_0 = 0.71$

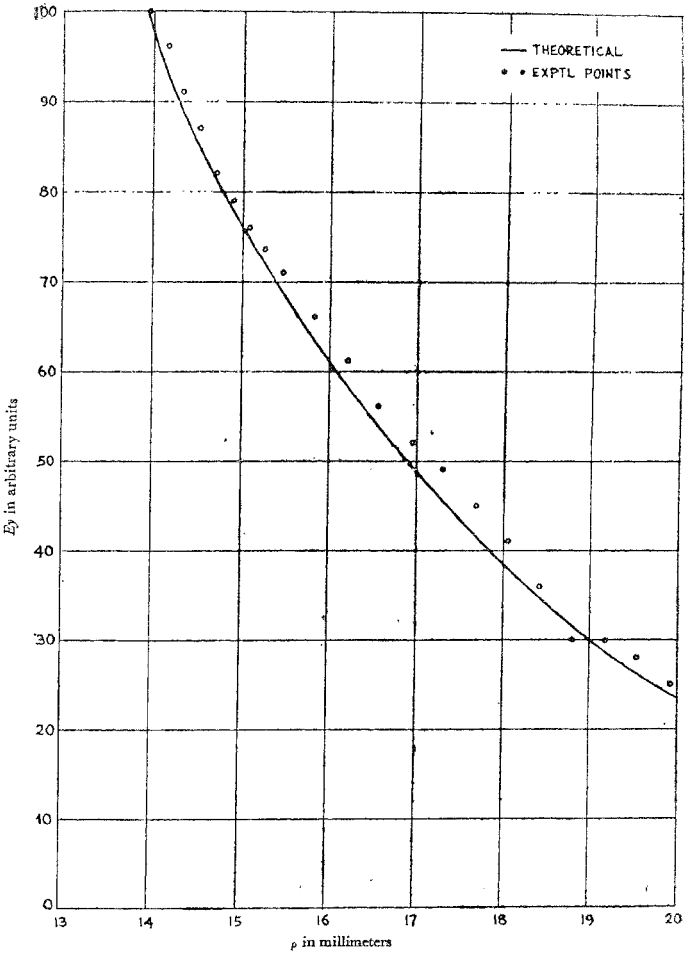


FIG. XV

Field spread outside the dielectric rod $B_5$ ; $\epsilon_r = 2.62$, $(2a/\lambda_0) = 0.82$

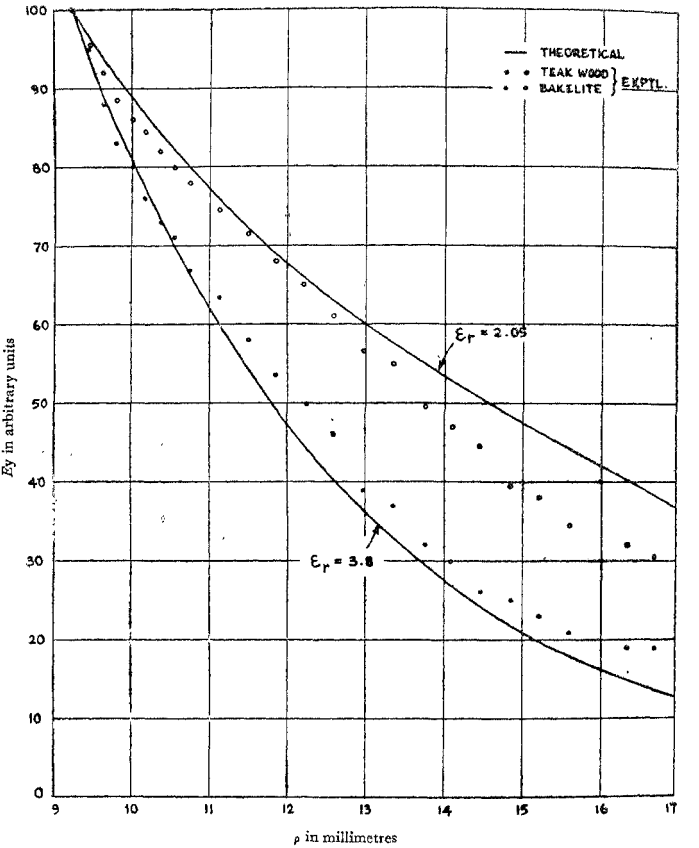


FIG. XVI

Field spread outside dielectric rods A and C

$2a/\lambda_0 = 0.51$

RADIATED FIELD AT A POINT ON THE AXIS OF THE DIELECRIC ROD

The experimental set up at the transmitting and receiving ends to measure the radiated field at a point on the axis ($\theta = 0°$) of the dielectric rod is shown in plates II and III respectively. The dielectric rod $B_2$ ($\epsilon = 2.62$, $2a/\lambda_0 = 0.51$) was used as a transmitting antenna and a pyramidal horn was used as a receiving antenna.

The experiment consisted of measuring the change in the power received when radiation from portions of the free end of the dielectric rod was suppressed by covering them with tin foil discs and rings described in Appendix 3. The change in power was measured by the precision attenuator method described earlier. The experiment was carried out for lengths of rod exposed ($l$) varying from .20 cms to 28 cms, in steps of 1 cm. The result of measurement are shown in Figs. XVII to XIX. The theoretical curves have been plotted only for $l = 23.3$ cms. This length was chosen because of simplicity in calculation arising out of the fact that the radiated fields due to the free end and cylindrical surface happen to be in phase. This simplifies the calculation as the two fields can be added algebraically to obtain the total field. The calculation has been made as follows:

At $\theta = 0°$, the radiated electric field $E_1$ due to the free end of the rod is

$$E_1 = f_1 f_2 = 2.35 \qquad [A]$$

The radiated elecric field $E_2$ due to the cylindrical surface of the rod is

$$E_2 = f_3 f_4 = 2.257\, l\, [\sin x/x]\, \exp.\, [j(x - \pi/2)]$$

where, $x = 0.2\ \pi l/\lambda_0$.

For $$l = 23.3 \text{ cms.}, \quad E_2 = 11.6 \qquad [B]$$

and is in phase with $E_1$. As only the ratio of powers is of ultimate interest we can write instead of $(A)$ and $(B)$

$$E_1 = 100;\ E_2 = 475, \text{ since } E_2/E_1 = 4.75.$$

The contribution from the free end involves the integral

$$\int_0^{k_1 a} k_1 \rho\, J_0(k_1 \rho)\, d(k_1 \rho) = E_1 \text{ (say)}$$

The contribution of the portion of the free end covered by a metal disc of radius $\rho$ would be ($\rho \leq a$)

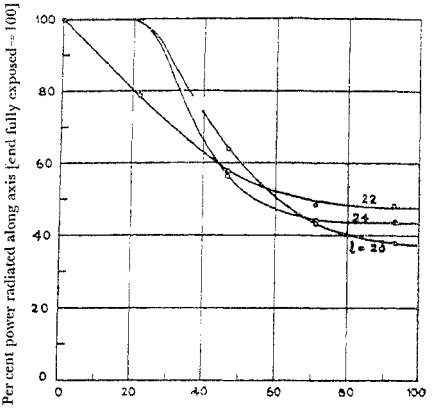


Per cent area of the free end covered

(*a*) Discs

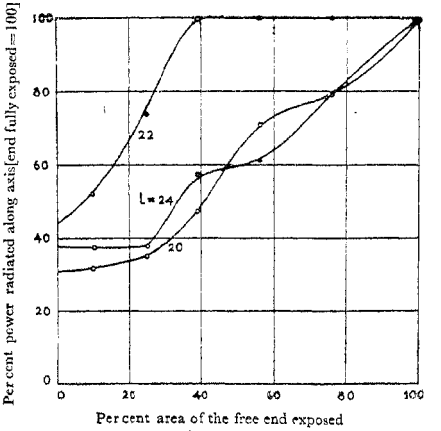


Per cent area of the free end exposed

(*b*) Rings

FIG. XVII

Effect of covering the free end of the rod *B* on radiation

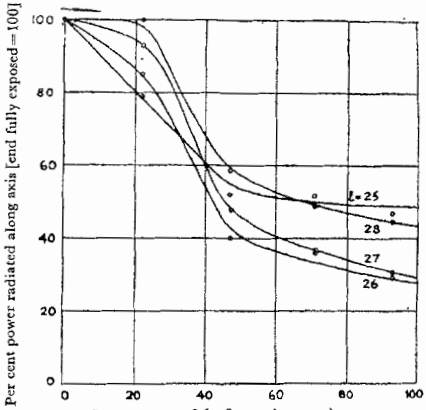


[*a*] Discs

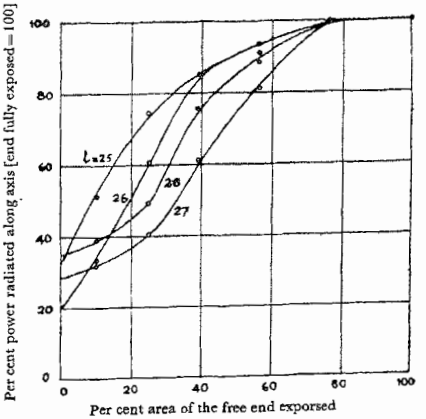


[*b*] Rings

FIG. XVIII

Effect of covering the free end of the rod $B_3$ on radiation

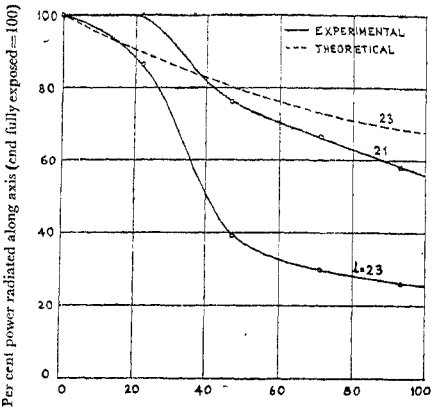


(*a*) Discs

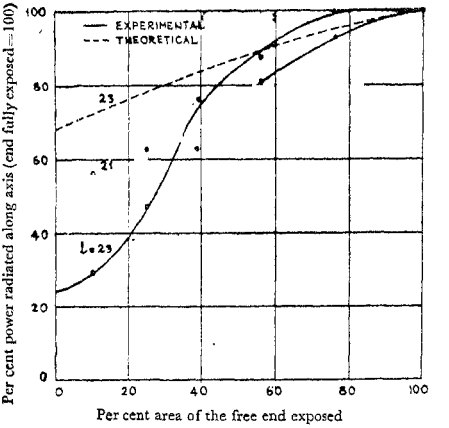


(*b*) Rings

FIG. XIX

Effect of covering the free end of the rod on radiation

$$\int_0^{k_1 \rho} k_1 \rho \, J_0(k_1 \rho) \, d(k_1 \rho) = \alpha \; E_1 \text{ (say)}.$$

The total power intensity obtained with the free end fully exposed is $(E_1 + E_2)^2$, but the power intensity with the free end covered with disc would $[(1-\alpha) E_1 + E_2]^2$ assuming that the metal disc fully suppresses the radiation from the covered portion leaving that from the exposed portion unaffected. The measured ratio of the powers should thus be equal to

$$[(1-\alpha) E_1 + E_2]^2 / (E_1 + E_2)^2.$$

Similarly, the fraction of power received along the axis when the free end is covered by a ring of internal radius $\rho$ and external radius $a$ would be

$$(\alpha E_1 + E_2)^2 / (E_1 + E_2)^2.$$

These fractions have been tabulated but are not reported here. Figs. XX and XXI show the variation of the fraction of power received with the length of the rod exposed when fixed areas of the free end are covered.

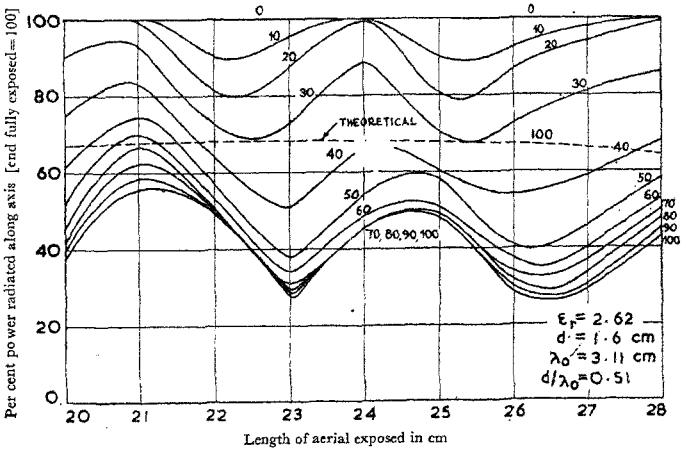


FIG. XX

Constant per cent area covered contours [discs]
Numbers on curves indicate per cent area of the end covered

It is observed that both theory and experiment indicate a reduction in the radiated power along the axis when the free end is covered, though the agreement between the two is not close. The difference may be due to experimental

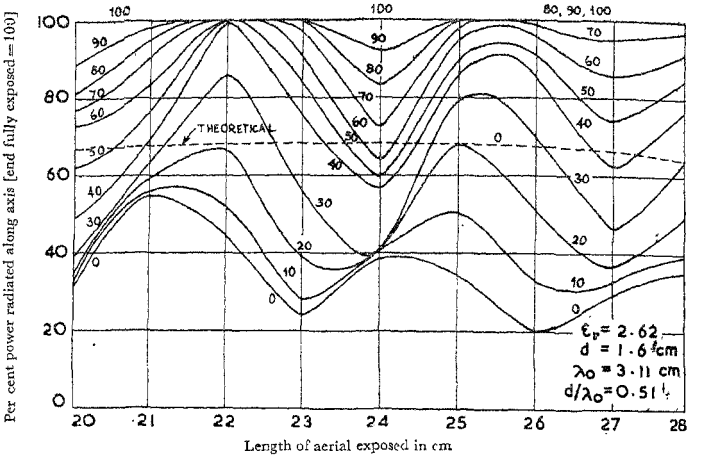


FIG. XXI

Constant per cent area exposed contours [rings]
Numbers on curves indicate per cent area of the end exposed

inaccuracy, errors in theoretical calculation. or input power variations caused by the mismatch which may appear due to varying the length of the aerial inside the mode transformer. The method of aerial fitting inside the mode transformer is the same as reported earlier[3]. The question of mismatch has been studied extensively and is reported in a separate paper. It is observed that the radiated power along the axis follows the same trend as the power transmitted by the dielectric rod. However, (Appendix 4) the reflected wave has negligible effect on the radiated field along the axis for the particular case. Hence the observed change in the radiated power along the axis is not due to the terminations giving rise to reflected waves on the dielectric rod but due to suppressing radiation from the covered portion. It is apparent from the foregoing discussions that both the free end of the rod as well as the cylindrical surface radiate energy as assumed in deriving the expression for the radiated field.

## Discussion

The unique feature of the present approach is the assumption that both the free end and the cylindrical surface radiate. Though radiation from the free end may be relatively small, it cannot be ignored altogether as it would be significant in determining the detailed structure of the radiation pattern. The approach ' which regards radiation as arising entirely out of the infinite plane at the free end raises several difficulties. It assumes that the $HE_{11}$ field distribution is valid everywhere on the plane which is not true at large distances from the rod. Also the validity of approximations made in the distance '$R$' while calculating the radiated field is doubtful if the aperture extends to infinity. These difficulties are obviated in the present approach by considering the source fields on a finite area comprising the free end and the cylindrical surface of the rod where the $HE_{11}$ mode of field distribution can be regarded as valid. If the cylindrical surface is not assumed to radiate, the observed dependence of radiation pattern on the length of the rod becomes difficult to explain. It is sought to be be explained[6] by the ad hoc assumption that the feed end of the rod radiates. But neither the magnitude of radiation from the feed end nor the directional characteristic has been evaluated. Theories[1,2] based on radiation from the cylindrical surface explain the dependence of the radiation pattern on the length with a fair degree of success. Methods[9,10] of controlling radiation from the cylindrical surface have also been described in literature. The experiments described in the present paper also show that radiation takes place from both the end as well as the cylindrical surface. Though the actual radiation patterns obtained experimentally and theoretically have not been compared here, the basic assumptions of the present approach have been verified.

## Appendix 1

(i) Sample numerical calculations: The inequality $k_1^2 > 0 > k_2^2$.

Consider $\epsilon = 2.62$, $2a = 1.60$ cms, $\lambda_0 = 3.11$ cms, $l = 20$ cms. From graphs given in Ref. 7, $\beta/k = 1.20$, $k = 2.020\ \text{cm}^{-1}$. So, $\beta = 2.424\ \text{cm}^{-1}$. The wavelength of the guided wave $\lambda_g = 2\pi/\beta = 2.59$ cm, $k_1 = 2.195\ \text{cm}^{-1}$, $k_2 = j\,1.34\ \text{cm}^{-1}$. So, the inequality assumed that $k_1^2 > 0 > k_2^2$ is justified.

(ii) The value of $G$:

$$k_0 = 1.34\ \text{cm}^{-1}; \quad G \approx 0.926; \quad G' = 1.685.$$

The error introduced by approximating $G'$ to $G$ is small as a slight error in the source fields does not give rise to appreciable error in the radiated fields.

(iii) Total field at $\theta = 0°$:

$$C_1 = jC\ 0.4866; \qquad C_4 \omega \mu = C 0.9356;$$
$$C_2 = C 0.3410; \qquad u = 1.616 \sin\theta.$$
$$C_3 \omega \mu = -jC 1.274;$$

Therefore,

$f_1 = 4.444\,\text{cm}^{-1}$; $f_3 = 2\ 257\,\text{cm}$;

$f_2 = 0.529\,\text{cm}$; $f_4 = 3.88 \exp.(j\,321.5^\circ)\,\text{cm}$.

The total field [eq. 22] = 10.7

The field has been expressed as a dimensionless quantity as is usual in the case of radiation pattern.

## APPENDIX 2

Description of dielectric rods used in experiments (Fig. III)

$L = 43.4$ cms $b = 6.4$ cms.

| Rod No. | Material | Diameter, $2a$ (cms) | |
|---|---|---|---|
| $A$ | Teakwood | 2.05 | 1.60 |
| $B_1$ | Perspex | 2.62 | 1.27 |
| $B_2$ | Perspex | 2.62 | 1.60 |
| $B_3$ | Perspex | 2.62 | 1 90 |
| $B_4$ | Perspex | 2.62 | 2.22 |
| $B_5$ | Perspex | 2.62 | 2.54 |
| $C$ | Bakelite | 3.80 | 1.60 |

## APPENDIX 3

Tin foil discs employed to cover the free end of the rod

Rod $B_2$ ($2a = 1.60$ cms.)

| Disc No. | Diameter mm | Area of disc Sq. mm | Area of the free end of the rod sq. mm | Area of the free end covered % |
|---|---|---|---|---|
| 1 | 7.5 | 44 | 200 | 22 |
| 2 | 11.5 | 95 | 200 | 47 |
| 3 | 13.5 | 143 | 200 | 71 |
| 4 | 15.5 | 188 | 200 | 94 |

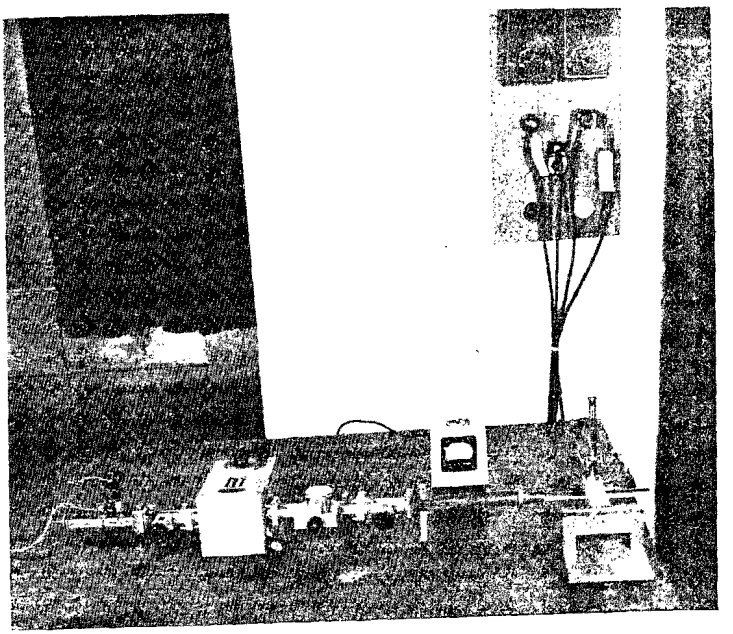

PLATE I

Measurement of field near the dielectric rod

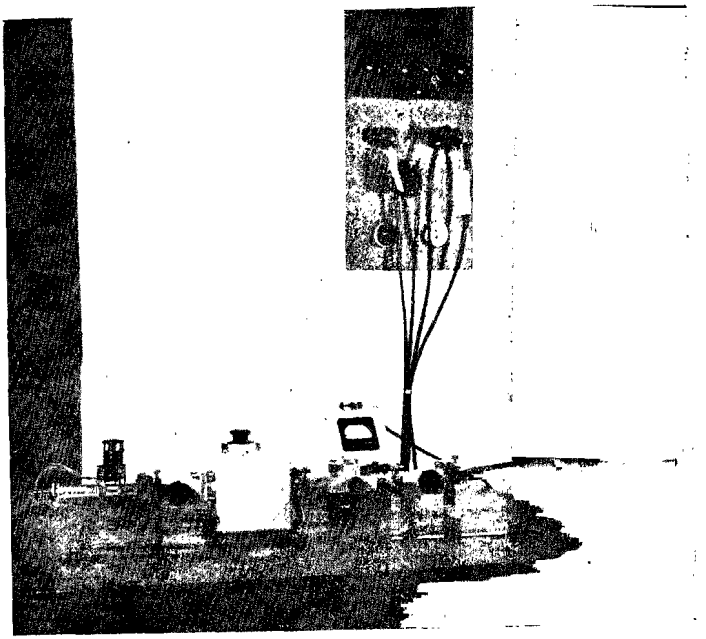

PLATE II

Measurement of radiated field: Transmitting side

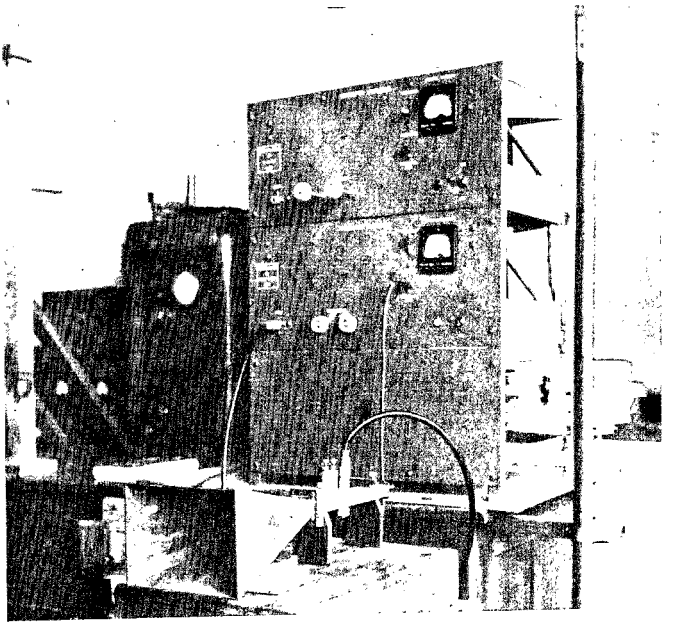

PLATE III

Measurement of radiated field : Receiving side

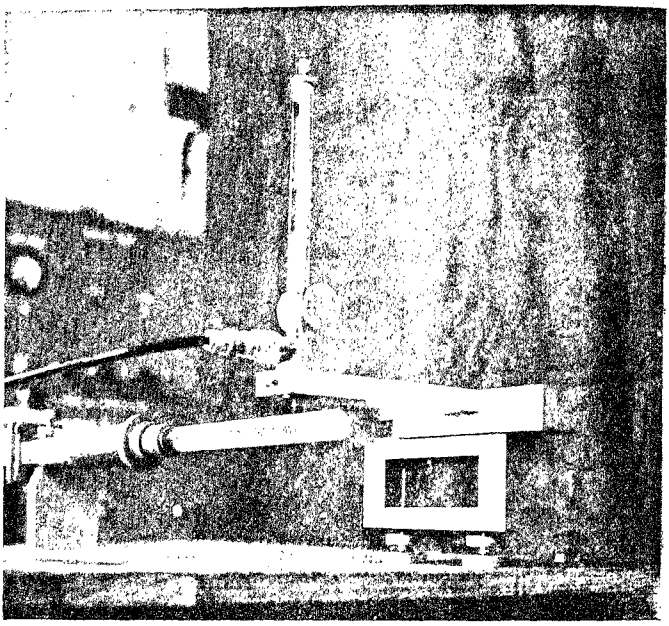

PLATE IV
Close-up view of the probe carriage

Tin foil rings employed to cover the free end of the rod : $B_2$ ($2a$=1.60 cms).

| Ring No. | Inner diameter (mm) | Outer diameter (mm) | Area of the free end exposed (Sq. mm) | Area of the free end exposed (Sq. mm) | Area of the free end exposed % |
|---|---|---|---|---|---|
| 1 | 14 | 16 | 154 | 200 | 77 |
| 2 | 12 | 16 | 113 | 200 | 56 |
| 3 | 10 | 16 | 78 | 200 | 39 |
| 4 | 8 | 16 | 50 | 200 | 25 |
| 5 | 5 | 16 | 20 | 200 | 10 |

## Appendix 4

*Effect of reflected wave on the radiated field :*

While calculating the radiated field, the presence of reflected wave was not considered in the expression for source fields. The presence of reflection would give rise to additional terms in the source field involving the factor $r$ exp. $(j\beta z)$, where, '$r$' is the reflection coefficient. This would affect the term $E_2$ while the forward wave gives rise to the factor.

$$\frac{\sin[l(\beta - k\cos\theta)/2]}{l(\beta - k\cos\theta)/2}$$

the reflected wave give rise to the additional factor

$$\frac{r\sin[l(\beta + k\cos\theta)/2]}{l[\beta + k\cos\theta]/2}$$

The error in the radiated field $E_2$ calculated by neglecting the reflected wave depends on the actual values of $l$ and $\theta$.

In the case of rod $B_2$ for $l = 23.3$ cms., $\theta = 0^\circ$ when $l(\beta - k\cos/\theta)/2$ is equal to $3\pi/2$, the fractional error in $E_2$ is seen to be

$$\frac{r\sin[l(\beta + k\cos\theta)/2]\,(\beta - k\cos\theta)}{\sin\{[l(\beta - k\cos\theta)/2]\,(\beta + k\cos\theta)\}}$$

which is $< r(\beta - k)/(\beta + k)$. The reflection coefficient $r < 1$ and $\beta \simeq k$. Hence, the effect of reflected wave on the radiated field in this particular case is negligible.

ACKNOWLEDGMENT

The authors express their grateful thanks to Prof. S. V. C. Aiya for the encouragement and facilities given during the course of investigation.

REFERENCES

1. Chatterjee, R. and Chatterjee, S. K. : . *J. Indian Inst. Sci.*, 1956, **38**, 93.
2. ——— ——— . . *Ibid*, 1957, **39**, 134.
3. Rama Rao, B., Chatterjee, R. and Chatterjee, S. K. . . *Ibid*. 1957, **39**, 143.
4. Chatterjee, R. and Chatterjee, S. K. . . *Jour. I.T.E.*, 1958, **3**, 280.
5. Schelkunoff, S.A. . . *Bell. System Tech. J.* 1936, **15**, 93.
6. Brown, J. and Spector, J. O. . . *Pro. I.E.E.*, 1957, **104**, Part B, 27.
7. Rama Rao, B. . . *J. Indian Inst. Sci.*, 1959, **41**, 23.
8. Muller, G. E. and Tyrell, W.A., . . *Bell. System Tech. J.*, 1947, **26**, 837.
9. Mueller, G. E. . . *Proc. I.R.E.*, 1952, **40**, 71.
10. Duncan, J. W. and Duhamel, R. H. . . *I.R.E. Trans.*, 1957, AP-**5**, 284.